Controlling Quantum Wave Packet of Electronic Motion on Field-Dressed Coulomb Potential of H$_2^+$ by Carrier-Envelope Phase-Dependent Strong Field Laser Pulses

Mohammad Noh Daud[1, a)]

Department of Chemistry, University of Malaya, 50603 Kuala Lumpur, Malaysia

Solving numerically a non-Born-Oppenheimer time-dependent Schrödinger equation to study the dissociative-ionization of H$_2$ subjected to strong field six-cycle laser pulses ($I = 4 \times 10^{14}$ W/cm^2, $\lambda = 800$ nm) leads to newly ultrafast images of electron dynamics in H$_2^+$. The electron distribution in H$_2^+$ oscillates symmetrically with laser cycle with $\vartheta + \pi$ periodicity and gets trapped between two protons for about 8 fs by a Coulomb potential well. Nonetheless, this electron symmetrical distribution begins to gradually break up for the H$_2^+$ internuclear separation larger than 9 a.u. in the field-free region at a time duration of 24 fs as a result of the distortion of Coulomb potential where the ejected electron preferentially localizes in one of the double-well potential separated by the inner Coulomb potential barrier. Moreover, controlling laser carrier-envelope phase ϑ enables one to generate the highest total asymmetry A_e^{tot} of 0.75 and -0.75 at 10° and 190°, respectively, associated with the electron preferential directionality being ionized to the left or the right paths along the H$_2^+$ molecular axis. Thus the laser-controlled electron slightly reorganizes its position accordingly to track the shift in the position of the protons despite much heavier the proton's mass.

Keywords: laser pulse, time-dependent Schrödinger equation, electronic state, wave packet, Coulomb potential

I. INTRODUCTION

The interaction of atoms and molecules with light has been extensively studied along with the significant progress in ultrafast optics.[1–10]. Short laser pulses with duration in the femtosecond time regime are readily accessible having electric field strengths of the order of the atomic unit of laser intensity $I_a = 1/2\epsilon_0 c |E_a|^2 = 3.5 \times 10^{16}$ Wcm^{-2}. $E_a = 5 \times 10^9$ Vcm^{-1} which is the strength of the Coulomb field experienced by an electron interacts with a nucleus in the ground state of the hydrogen atom. On the application of a strong field whose strength is comparable to the Coulomb interaction between electrons and nuclei in atoms or molecules, it is strong enough to compete with the Coulomb forces in steering the dynamics of electrons. This leads to the discovery of a great number of new strong-field phenomena such as the above-threshold ionization[11,12], the above-threshold dissociation[13,14], the above-threshold Coulomb explosion[15], and the high-harmonic generation[11,16–19].

The high harmonic generation opens a new route to produce XUV sub-femtosecond and attosecond laser pulses with the maximum photon energy calculated classically by $E = I_p + 3.17U_p$[16], where $U_p = e^2 E_0^2/4m\omega^2 = e^2 I/4m\omega^2$ is the ponderomotive potential corresponding to the cycle-averaged kinetic energy of a free classical electron in the oscillating electric field at an angular frequency ω, acting as a potential to eject the electron from a region of peak intensity I, and I_p is the zero-field ionization potential[16,20]. As a non-perturbative nonlinear process, high harmonic generation has opened up a whole new research area such as

———
a)Electronic mail: mnoh@um.edu.my; Author to whom correspondence should be addressed.

femtochemistry and attoscience in measuring the dynamics of electron and nucleus on their natural time scales[1,21–23]. It can be well understood qualitatively in the framework of a semi-classical three-step model[20].

The control of the electronic population with a strong field has been always one of the main aims in ultrafast science[1,21–23] and currently an active area of research because of its potential application in controlling chemical reactions. In common practice, to control the populations arises from the ability to control generally the electric field rather than the envelope of a laser pulse. Several experimental schemes have been implemented to study the carrier-envelope phase effects in dissociative ionization of molecules H$_2^+$/HD$^+$[24] and H$_2$/D$_2$[25–28], and in the ionization of atoms Kr[29] and Rb[30]. Moreover, extensive theoretical calculations using such as the time-dependent methods on two field-coupled electronic potentials of H$_2^+$/HD$^+$ have been performed to understand the underlying process of the laser-controlled electron motion[31–35]. The dependence of the electron asymmetry of above-threshold ionization on the carrier-envelope phase of few-cycle pulses for atoms has been studied theoretically[31–35]. The dependence of the angular distribution of electrons on the carrier-envelope phase of circularly polarized few-cycle pulses has been investigated for symmetric molecules[36]. Further theoretical works have been performed to investigate the carrier-envelope phase dependence in molecular isomerization[37–41] and high harmonic generation[42].

As the simplest molecule with electron interaction in nature, I chose the hydrogen molecule H$_2$ that provides a unique system for studying molecules in strong laser fields[5,43,44]. The aim to resolve vibrational and electronic dynamics in H$_2$ hence has set off two branches of advancement in shorter laser pulses and imaging techniques. In this work, a pulse with a wavelength of 800 nm excites H$_2$ molecule from a specific vibrational level

of its ground electronic state $X^1\Sigma_g^+$ to a level leading to above-threshold ionization when the ionized electron keeps absorbing further photons. Here, I report the realization of such actively control field over the electron dynamics in H_2 and its ionization product H_2^+ by numerically simulating the time-dependent Schrödinger equation with a full range of the carrier-envelope phase of the laser field[45]. As a result, I can quantify the newly electron localization on either side of the nuclei during dissociation of H_2^+.

II. THEORY

Within a non-Born-Oppenheimer formalism, I write a complete multi-dimensional time-dependent Schrödinger equation for the H_2 molecule in a linearly polarized laser field as[46]

$$i\frac{\partial \psi(z_1, z_2, R, \vartheta, t)}{\partial t} = \hat{H}\psi(z_1, z_2, R, \vartheta, t) \quad (1)$$

$$\hat{H} = -\frac{1}{m_N}\frac{\partial^2}{\partial R^2} - \frac{1}{2}\left(\frac{\partial^2}{\partial z_1^2} + \frac{\partial^2}{\partial z_2^2}\right) + \frac{1}{R}$$

$$-\frac{1}{\sqrt{(z_1 - R/2)^2 + a}} - \frac{1}{\sqrt{(z_1 + R/2)^2 + a}}$$

$$-\frac{1}{\sqrt{(z_2 - R/2)^2 + a}} - \frac{1}{\sqrt{(z_2 + R/2)^2 + a}} \quad (2)$$

$$+\frac{1}{\sqrt{(z_1 - z_2)^2 + b}} + E(\vartheta, t)(z_1 + z_2)$$

where m_N is the mass of a nucleus, R is the relative H-H internuclear distance, z_i is the coordinate of an electron i with respect to the nuclear center of mass, $a = 0.7$ and $b = 1.2375$ are parameter values chosen for the soft-core Coulomb potential to reproduce accurately the first three Coulomb potentials of H_2.

The laser-molecule interaction potential is given by $E(\vartheta, t)(z_1 + z_2)$ that induces a time-dependent radiative coupling. In a dipole approximation and Coulomb gauge, I derive the laser field $E(\vartheta, t)$ from a vector potential to give[46]

$$E(\vartheta, t) = \epsilon(t)\cos[\omega t + \vartheta] + \frac{\sin[\omega t + \vartheta]}{\omega}\frac{\partial}{\partial t}\epsilon(t) \quad (3)$$

where ω is the laser angular frequency, ϑ is the carrier-envelope phase and ϵ is the envelope function for a few-cycle laser pulse in the form of

$$\epsilon(t) = \sqrt{\frac{I}{I_a}}\cos^2\left[\frac{\pi t}{t_{tot}}\right],$$

where t_{tot} is the pulse duration. Fig. 2 shows the six optical cycles laser pulse as a function time (in fs) with its maximum amplitude at $t_{tot} = 8$ fs.

The laser control parameters can be set differently, depending on the selected laser pulse wavelength and shape of the electric field such as previously experimental set-up of carrier-envelope phase controlled laser field composed of 800 nm pulse[47], two-color laser field consisted of 400 nm/800 nm pulses[27], mid-IR two-color field composed of 900 nm/1800 nm pulses[48], and mid-IR carrier-envelope phase controlled laser field with 2100 nm pulse[49]. With the chosen wavelength $\lambda = 800$ nm, I calculate the laser parameters of frequency $\omega = 45.56/\lambda = 0.057$ a.u., period $\tau = 2\pi/\omega = 2.67$ fs, electron ponderomotive radius $\alpha = \sqrt{I/\omega^4 I_{au}} = 33$ a.u., and ponderomotive energy $U_p = I/(2\omega)^2 = 0.88$ a.u..

Numerically solving for equation (1) requires the electronic-nuclear wave packet ψ to be propagated with time intervals $[t, t+\Delta t]$. I achieve this using the second-order split operator technique[46,50] as follows

$$\psi(z_1, z_2, R, \vartheta, t + \Delta t)$$

$$= \exp\left(-i\hat{H}\Delta t - iV_{damp}\Delta t\right)\psi(z_1, z_2, R, \vartheta, t)$$

$$\approx \exp\left(-iV_{damp}\frac{\Delta t}{2}\right)\exp\left(-i\hat{H}\Delta t\right)\exp\left(-iV_{damp}\frac{\Delta t}{2}\right)$$

$$\times \psi(z_1, z_2, R, \vartheta, t)$$

$$(4)$$

by adding a damping potential V_{damp} and a time-step of $\Delta t = 3.4475$ a.u. is used. In order to propagate the wave packet in time, equation (4) requires repeated operations of the exponential time evolution operator on $\psi(z_1, z_2, R, \vartheta, t)$ on an equally electron spaced grid of size $-254 \leq z_i \leq 254$ a.u. consisting of 1008 grid points for each electron and a nuclear spaced grid of size $0 \leq R \leq 48$ a.u. consisting of 320 grid points. I chose the grid size in such a way that its size exceeded the maximum electron excursion α. Some portions of the dissociating wave packet will eventually reach the boundary of the numerical grid and unphysically reflected back onto the grid. In order to prevent such reflection, I employ the following complex damping potential[36,46,51–53]

$$V_{damp}(\Gamma) = \begin{cases} 0.0 & ; \ \Gamma < \Gamma_{damp} \\ -iA_{damp}\ln\left[\cos\left(\frac{\Gamma - \Gamma_{damp}}{\Gamma_{max} - \Gamma_{damp}}\right)\right] & ; \ \Gamma_{damp} \leq \Gamma \leq \Gamma_{max} \end{cases}$$

With this scheme, the damping Γ_{damp} is turn on at $R_{damp} = 40$ a.u. and $z_{damp} = \pm 246$ a.u. which Γ_{max} represents the size of the grids for R and z, while I optimize the dimensionless parameter A_{damp} to give the strength of the damping. I have verified that the absorber led to only a few percent loss of the norm near the end of the pulse.

Both of the H_2 and H_2^+ molecules do not have a permanent dipole moment. The dipole exists when it is induced through the coupling between its electronic states and the electric field. The coupling is non-perturbative and nonlinear processes. On top of that the promotion of H_2 to H_2^+ strongly depends on the parallel alignment of the molecular axis with respect to the elec-

tric field polarization vector. Therefore, the promotion must subject to upon an initial electronic-nuclear wave packet[51–53] consisting of g symmetry-type electronic wave function:

$$\psi(z_1, z_2, R, \vartheta, t = 0) = \mu_z(\vartheta, t)\psi_i(z_1, z_2, R) \quad (5)$$

where

$\mu_z(\vartheta, t) = \langle \psi(z_1, z_2, R, \vartheta, t) | (z_1 + z_2) | \psi(z_1, z_2, R, \vartheta, t) \rangle$ is the z-component of the laser-induced transition dipole moment connecting the electronic states, and the evolution of ψ as the electronic-nuclear ground state wave function for H_2 starting from $t = 0$ propagated in time using equations (4). Generally, I write $\psi_i(z_1, z_2, R)$ as a product of electronic and nuclear Born-Oppenheimer wave functions,

$$\psi_i(z_1, z_2, R) = \sigma_g(z_1, z_2 : R)\psi_{g,v}(R : E_i) \quad (6)$$

where σ_g is the electronic wave function parametrically depending on all nuclear degrees of freedom R and $\psi_{g,v}$ is the eigenfunction (represents the bound-state nuclear wave function) of the time-independent Schrödinger equation[51–53]

$$\left\{ -\frac{1}{m_N}\frac{\partial^2}{\partial R^2} + V(z_1, z_2 : R) \right\} \psi_{g,v}(R) = E_v \psi_{g,v}(R) \quad (7)$$

in the electronic state with energy E_i. One-electron wave function σ_g for H_2^+ is shown in Fig. 1 and can also be obtained from equation (9) at $t = 0$ fs.
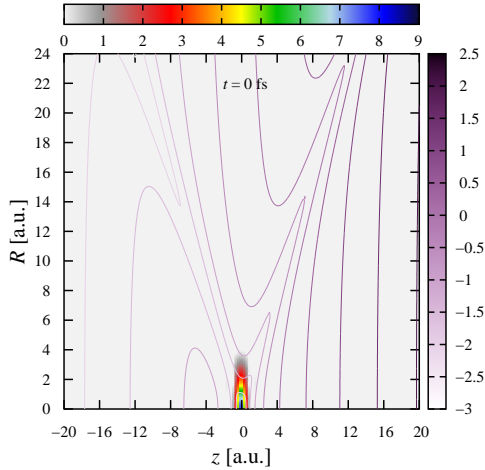

FIG. 1. (i) The evolution of the one-electron nuclear wave packet $\sigma_g(z_i)$ or Φ'_e (in arbitrary unit) of H_2^+ as a function of z and R at fixed of $\vartheta = 0°$ and $t = 0$ fs calculated using equation (6) or (9); (ii) The superimposed of one-electron Coulomb potential (in a.u.) of H_2^+ as a function of z and R at a fixed of $\vartheta = 0°$ calculated using equation $-1/\left[(z_1 - R/2)^2 + a\right] - 1/\left[(z_1 + R/2)^2 + a\right] + z_1 E(\vartheta, t)$ appears in equation (2). The initial nuclear wave function $\psi_{g,v}$ in equation (6) is in the vibrational energy level of $v = 3$ following the first ionization of H_2 molecule[54].

III. RESULTS

A. Electronic wave packet dynamics of H_2^+

In the following discussions, I address the details mechanism to understand the ultrafast electron dynamics of H_2^+ by analyzing directly the calculated two-electron nuclear wave packet $\psi(z_1, z_2, R, \vartheta, t)$. The main parameter to be concerned is the carrier-envelope phase of the laser field in steering the electron. The current non-Born-Oppenheimer calculation allows me to take the electron and nuclei into account to describe both the ionization and dissociation steps concurrently. It is important to note that the rotational motion of the molecule with respect to the polarization of the electric field is a relatively slow process, which occurs on the picosecond timescale. While, the electron motion occurs faster than the femtosecond timescale, and hence, the rotational motion can be presumably frozen.

Following a radiative coupling of σ_g and σ_u states, their coherent superposition leads to the electron localization on either side of H_2^+ depending on the phase of the laser field. I monitor the one-electron localization in the time domain based on the following wave packet evolution

$$\Phi_e(z_1, \vartheta, t) = \int_0^{R_0} dR \left\{ \int_{-\infty}^{-z_0} dz_2 \, |\psi(z_1, z_2, R, \vartheta, t)|^2 \right.$$
$$\left. + \int_{z_0}^{\infty} dz_2 \, |\psi(z_1, z_2, R, \vartheta, t)|^2 \right\} \quad (8)$$

by integrating out over the nuclear coordinate R and the ionized electron coordinate z_2 from the ionization of H_2 in the continuum is subjected only to the laser field and does not feel the influence of the Coulomb potential any longer. This electron follows the oscillation of the laser field where its classical maximal displacement is defined by α and with the applied intensity and wavelength, the electron travels up to 1.75 nm away from its parent ion. I consider $z_0 = 33$ a.u. to represent the single ionization of electron where z_0 is the distance of the electron from the center of mass of H_2.

In equation (8), I consider $R_0 = 2, 3$ a.u. to represent H_2^+ near its equilibrium separation in which the electronic wave packet dynamics is primarily diabatic, $R_0 = 4$ a.u. to represent H_2^+ near the two lowest field-dressed degenerate states σ_- and σ_+ in which the dynamics is primarily adiabatic and $R_0 = 5, 6, 7, 8$ a.u. to represent H_2^+ at the dissociation channel where the dynamic is the mixture of adiabatic and diabatic[54]. Based on the two lowest electronic states σ_g and σ_u of H_2^+, I can monitor the one-electron nuclear wave packet with specific ϑ against time as follows

$$\Phi'_e(z_1, R, \vartheta, t) = \sigma_-^a(z_1, R) \int_{-\infty}^{-z_0} dz_2 \psi(z_1, z_2, R, \vartheta, t_f)$$
$$+ \sigma_+^a(z_1, R) \int_{z_0}^{\infty} dz_2 \psi(z_1, z_2, R, \vartheta, t_f) \quad (9)$$

where $\sigma_\pm^a$ are defined by

$$\sigma_\pm(z_1, R) = \frac{1}{\sqrt{2\pi}}\left[\sigma_g(z_1, R) \pm \sigma_u(z_1, R)\right] \quad (10)$$

It is assumed that $\sigma_g > 0$ everywhere and $\sigma_u > 0$ at $z_1 > 0$, $z_1 \approx R/2$. In the absence of an external field, σ_+ and σ_- levels are always degenerate.

During a molecule rearrangement, the motion of the nuclei can be followed by a reorganization of the electronic structure. It is the motion of the nuclei that sets the time scale of 10^{-14} s because the electronic reorganization on the 10^{-17} s exactly tracks the shifts in the positions of the nuclei. Therefore, it is often unjustified to approximate that electronic and nuclear motion are decoupled from one another. In this works of the multidimensional electronic-nuclear wave packet, I use equation (8) to set the dynamics of the nuclei to be frozen around which the electron evolves. At a particular nuclear configuration, a single laser pulse attempts to reorganize the electronic wave packet Φ_e so that the electron distributes according to the laser-dressed Coulomb potential landscape. To relate the instantaneous adjustment of the electron with the position of the nuclei, I carry out comparative studies with the one-electron nuclear wave packet derived from equation (9). I keep the carrier-envelope phase of both equations (8) and (9) fixed at $\vartheta = 0°$.

Figure 2 shows the electronic wave packet Φ_e in relation with the potentials σ_g and σ_u, immediately after the first ionization of H_2. The initial Φ_e is characterized by one node separating the two peaks, which are the position of the protons. The Φ_e accelerates towards the equilibrium separation of H_2^+, $R = 2$ a.u., associated with a small region of the squeezed orbitals in the laser field. Figure 2 depicts the evolution of Φ_e by setting up $R_0 = 2$ in equation (8). Even though the electron feels substantial attraction from both protons at this R, most of its time being delocalized in the laser field due mainly to accommodate the localized periodic field.

As the R increases, the Φ_e spreads faster over the laser cycle when it traverses the laser focus located at the center of the six-cycle pulse at a time duration of 8 fs. Comparing the wave packets when I set up $R_0 = 3$ and $R_0 = 4$ a.u, the electron distribution shows slight discontinuation around the laser focus. This indicates the electron continuously gaining energy from the field to accelerate as it passes the laser focus. The critical internuclear distance at $R = 4$ is the location of two-photon crossing of the field-dressed diabatic potentials for the σ_g and σ_u states. The detailed discussion on the potentials can be found in reference (54)[54]. The crossing creates a potential barrier for the lower state σ_g. It approximately coincides with the position after the Φ_e passing through the laser focus. Thus the acceleration can be attributed to the non-adiabatic phenomena of the electron tunneling through the barrier[54–58]. Other interesting phenomena from bond softening[59–66] and vibrational trapping[66–72] of H_2^+ in the proximity of the barrier has been extensively studied and successfully imaged recently reported in reference (54)[54].

Further analysis of Fig. 4 using equation (9) reveals that the one-electron nuclear wave packet Φ_e' begins to interact with the distorted Coulomb barrier formed by the electric field and the static Coulomb potential at a time duration of 8 fs which coincides with the laser focus. Experimentally, D_2 molecule takes 4 fs using sub-8
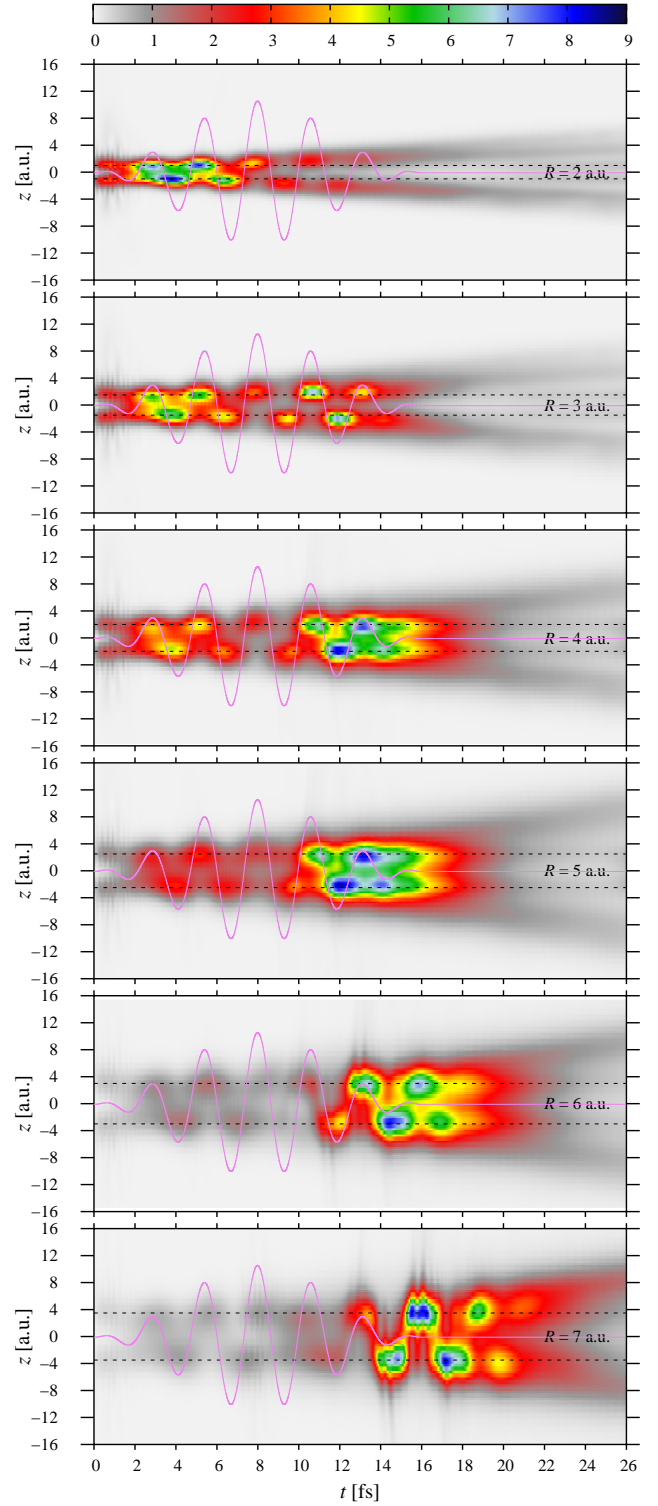

FIG. 2. (i) Evolution of the initial electronic wave packets Φ_e (in arbitrary unit) as a function of t and R for H_2^+ calculated using equation (8) with fixed of $t = 0$, $\vartheta = 0°$ and $R_0 = 2 - 7$ a.u. (ii) Six optical cycles laser field E (in arbitrary unit) as a function of t and ϑ calculated using equation (3) with fixed of $\vartheta = 0°$.

fs pulses to explode and significantly stretch the bond length[73,74]. The Coulomb barrier located between the two protons begins to appear around $R = 4$ a.u. illustrated by the superimposed contour map in Fig. 4.
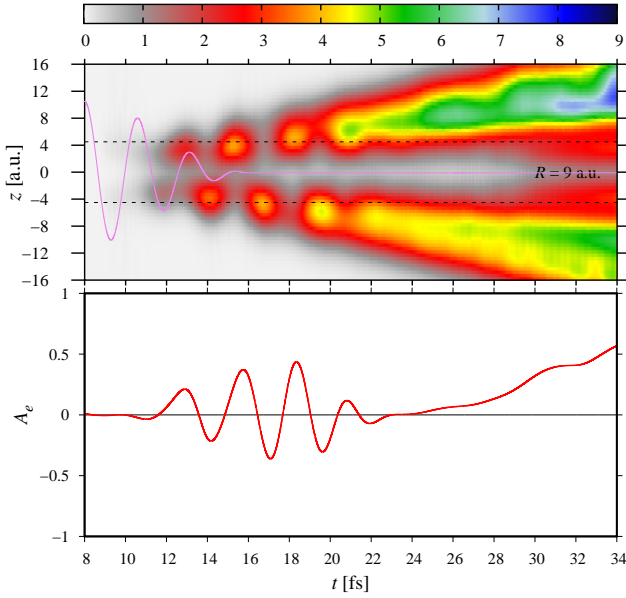
FIG. 3. Evolution of the initial electronic wave packets Φ_e (in arbitrary unit) as a function of t and R for H_2^+ calculated using equation (8) with fixed of $t = 0$, $\vartheta = 0°$ and $R_0 = 9$ a.u. (ii) Six optical cycles laser field E (in arbitrary unit) as a function of t and ϑ calculated using equation (3) with fixed of $\vartheta = 0°$ (iii) Electron asymmetry parameter A_e (dimensionless quantity) as a function of t and ϑ calculated using equation (11) with fixed of $\vartheta = 0°$.

In other words, the Φ_e' takes about 8 fs being trapped in the Coulomb potential well before entering the inner Coulomb barrier region consists of a double-well potential. This phenomenon can be also associated with vibrational trapping of the nuclear wave packet in the lowest σ_g state[54]. Up to this point, the electron distribution is symmetric with respect to the center of mass of H_2^+. After this point, the electron distribution splits into two ionization paths. As shown in Fig. 2, the electron involves the tunneling ionization after 8 fs being driven back and forth by the periodic electric field towards both right and left protons as the molecule stretches higher than 4 a.u.

As the electron to leave the laser focus for distances larger than $R = 4$ a.u., Fig. 2 displays the electron begins to concentrate at the end of the laser cycle to adjust its distribution according to the edge shape of the carrier-envelope phase. At this region of Rs, the electron has just passed through the barrier arising from the two-photon crossing[54]. Setting up $R_0 = 6$, the distribution begins to leave completely the laser focus and accelerates further into the field-free region. Apart from increasing in acceleration, the ejected electron traverses the laser focus rapidly quivering. Setting up $R_0 = 7$, the fast quivering electron can be seen in Fig. 2, which its distribution begins to split concentrated on both protons.

At $R = 9$ a.u, Fig. 3 depicts the Φ_e in the phase to leave the field where the electron begins to favorably stick on one of the protons, accompanied by the dissociation of H_2^+ to form either $H + H^+$ or $H^+ + H$. Looking back at Fig. 4, the electron distribution remains nearly

symmetric up to 12 fs. When the Φ_e' evolves after 16 fs, its distribution is clearly no longer symmetric after the molecule stretches longer than 9 a.u. Experimentally, this electron localization have been imaged in real time by using carrier-envelope phase controlled laser pulses from a Mach-Zehnder interferometer which allows to probe the electron localization in H_2^+ within 15 fs at an internuclear distance of about 8 a.u.[75]. In the separated atoms, the electron distribution is concentrated in two rather small regions about each nucleus. Thus as R stretches further, the kinetic energy of the ejected electron increases gradually in the field-free region. This is revealed in Fig. 4 as the bulk of distribution reaches 20 a.u. in just 36 fs at the right side of the molecule. It takes exactly the opposite path of the steepest-descent of the Coulomb potential. Noted that the region between the nuclei is classically forbidden for large R, but it is still accessible according to quantum tunneling.

As the H_2^+ molecule stretches to a longer R following ionization, it can reach a limit where the nuclei are too far apart and the electron-proton Coulomb attraction becomes too weak for binding, resulting in dissociation of H_2^+ to $H + H^+$. At large R where the Φ_e leaves completely the field, the coherent superposition of H_2^+ orbitals as σ_+ is presumably localized at the right proton H^+, $z_1 = R/2 > 0$ or as σ_- to be localized at the left proton H^+, $z_1 = -R/2 < 0$. In other word, the proton H^+ localizes at $z_1 < 0$ for σ_+ or at $z_1 > 0$ for σ_-. Thus as R increases and the H_2^+ orbitals are distorted, its Coulomb potential and the laser field form the inner barrier to further ionize H_2^+. This important nonlinear effect is a result of interference of two lowest H_2^+ states leading to charge resonance enhanced ionization[66,76–78]. For the strong-field ionization of such two-center H_2^+ molecule consisting of two Coulomb potential wells, the two most important orbitals $\sigma_\pm$ could be the highest occupied molecular orbital (HOMO) or the lowest unoccupied molecular orbital (LUMO). In particular, the effect of the phase-dependent resonance enhanced ionization on the ratio of electron localization between the two ionization channels is very important to be investigated. I will represent the ratio in terms of an asymmetry parameter in the following section.

B. Electron localization in H_2^+

In the absence of the electric field, the H_2^+ electron is not inherently predetermined moving on the left or the right along its molecular axis. However, the direction can be predetermined in the presence of the electric field provided that the gradient of the laser-dressed Coulomb potential is known beforehand. Various control experiments have been carried out for the last fifteen years to investigate the influence of parameters like pulse duration, intensity, wavelength, and polarization direction on either carrier-envelope phase control[47,79–81], or two-color control combined $\omega + 2\omega$ fields[27,48,82,83], or $\omega + 3\omega$[84], and also on the attosecond time-resolved electron dynamics in H_2[85].

As far as the most probable controlled direction of electron motion is concerned, one requires an asymme-
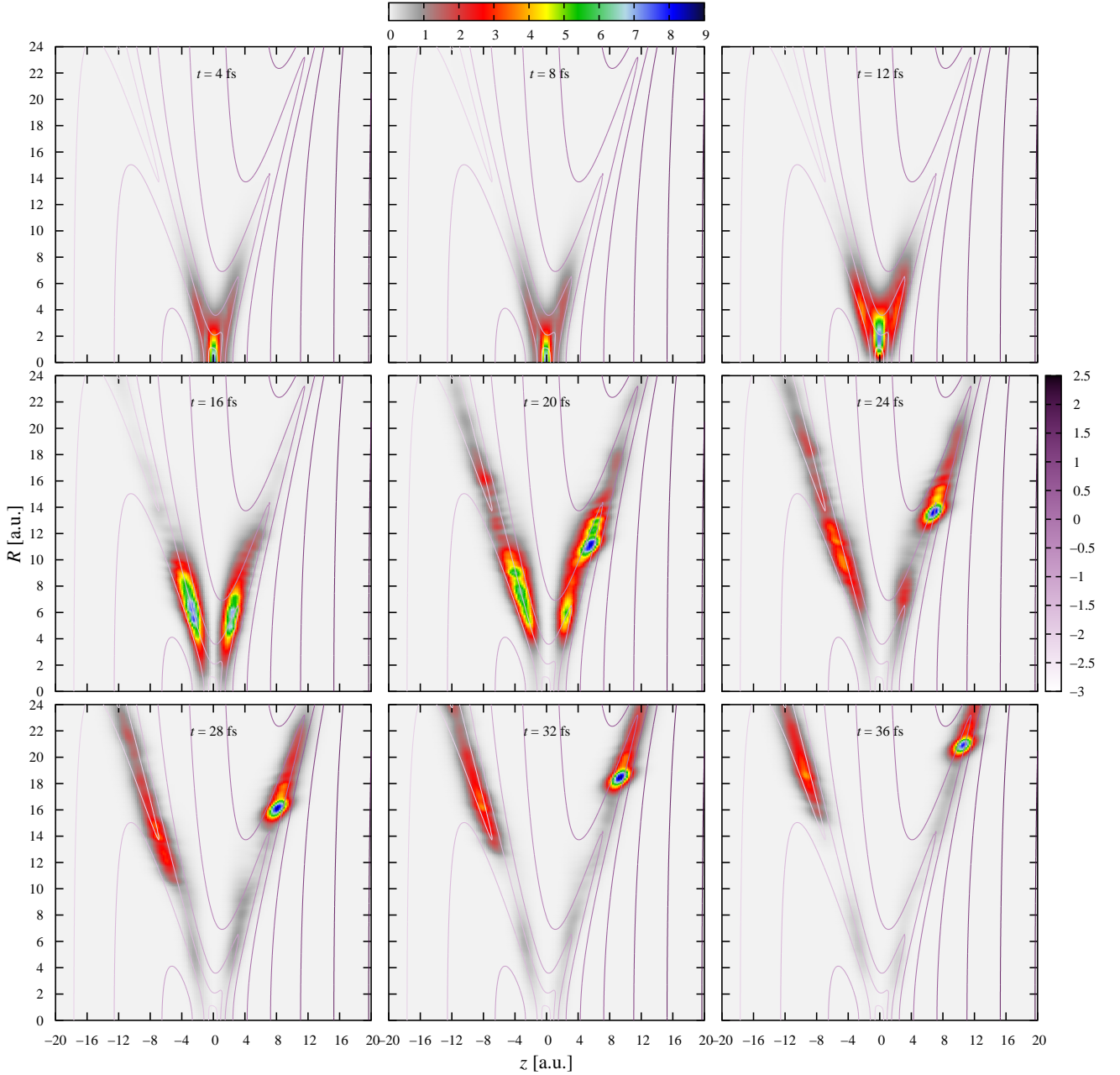
FIG. 4. (i) Evolution of the one-electron nuclear wave packets Φ'_e (in arbitrary unit) of H_2^+ as a function of z and R calculated using equation (9) with fixed of $\vartheta = 0°$ and $t = 4 - 36$ fs; (ii) Superimposed of one-electron Coulomb potential (in a.u.) of H_2^+ as a function of z and R with fixed of $\vartheta = 0°$ calculated using equation $-1/\left[(z_1 - R/2)^2 + a\right] - 1/\left[(z_1 + R/2)^2 + a\right] + z_1 E(\vartheta, t)$ as appears in equation (2).

try parameter A to quantify it, which I can express the temporal electron asymmetry for the wave packet evolution in Figs. 3 as follows

$$A_e(\vartheta, t) = \frac{P_e^+(\vartheta, t) - P_e^-(\vartheta, t)}{P_e^+(\vartheta, t) + P_e^-(\vartheta, t)} \quad (11)$$

by projecting the wave function $\psi(z_1, z_2, R, t)$ onto the electronic states in Eq. (10) where

$$P_e^\pm(\vartheta, t) = \int_{R_1}^\infty dR \left\{ \int_{-\infty}^{-z_0} dz_2 \, |\psi_\pm(z_2, R, \vartheta, t)|^2 \right. $$
$$\left. + \int_{z_0}^\infty dz_2 \, |\psi_\pm(z_2, R, \vartheta, t)|^2 \right\}, \quad (12)$$

$\psi_\pm$ are defined by

$$\psi_+(z_2, R, \vartheta, t) = \int_{-z_0}^0 dz_1 \sigma_+(z_1, R)\psi(z_1, z_2, R, \vartheta, t),$$
$$(13)$$

$$\psi_-(z_2, R, \vartheta, t) = \int_0^{z_0} dz_1 \sigma_-(z_1, R)\psi(z_1, z_2, R, \vartheta, t).$$
$$(14)$$

and $-1 \leq A_e \leq +1$ namely A_e equals 0 for equal electron distribution, and ± 1 for the highest degree of electron localization on the right or the left side of H_2^+ molecule, respectively. All the ϑ-dependent effects in

Eqs. (13) and (14) in general have been understood as resulting from the interference between two quantum channels corresponding to different numbers of absorbed photons[86]. In this perspective, ϑ control is a form of more general coherent control[27,87].

Figure 3 shows the newly electron asymmetry A_e monitored in time when H_2^+ stretches to 9 a.u. In the laser field, there is an almost perfect one-to-one correspondence between the A^{el} and the localization of the Φ_e concerning its ratio on the left and right sides of H_2^+. The electron direction is not preferentially localized in this region and the trend continues until it enters the field-free region with times duration exceeding 16 fs. The ejected electron preferentially localizes after 24 fs and its degree of localization keeps increasing with time. Comparing to the plot in Fig. 4 for the field-free evolution of Φ_e' at $t = 24$ fs, one observes that the one-electron wave packet in Fig. 3 becomes dominant in determining the localization of the entire H_2^+ molecule where the electron favorably localizes at the right side, while the proton oppositely localizes tracking the downwards direction of the Coulomb potential slope with kinetic energies ranging from 1.5 eV to 4.5 eV. So far, I have only considered the wave packet evolutions by setting-up $\vartheta = 0°$. I can investigate the variation of the asymmetry A_e for all ϑs by considering the above-threshold ionization spectra for $H_2^{+\,2,4,6-8}$.

The electron asymmetries for a such case can be calculated based on the following expression

$$A_e(\vartheta, E_e) = \frac{S_e^+(\vartheta, E_e) - S_e^-(\vartheta, E_e)}{S_e^+(\vartheta, E_e) + S_e^-(\vartheta, E_e)}. \quad (15)$$

where $S_e^\pm$ are the above-threshold ionization spectra for the H_2^+ electron localized on the right and left protons. For a series of ϑ, I can determine $S_e^\pm$ as the following

$$S_e^\pm(\vartheta, E_e) = \frac{1}{|p_e|} \int_0^\infty dR \int_{-z_0}^{z_0} dz_1 \left| \bar{\psi}_\pm(\vartheta, p_e, z_1, R) \right|^2 \quad (16)$$

where $E_e = p_e^2/2$ is the kinetic energy with its corresponding linear momentum p_e and $\bar{\psi}_\pm$ are the wave functions for electron evaluated at $z_0 > 200$ a.u. to allow the electron of H_2^+ to be ionized. Inserting Eq. (16) into Eq. (15), I obtain

$$A_e(\vartheta, E_e) = \int_0^\infty dR \int_{-z_0}^{z_0} dz_1$$
$$\times \left\{ \frac{\left| \bar{\psi}_+(\vartheta, p_e, z_1, R) \right|^2 - \left| \bar{\psi}_-(\vartheta, p_e, z_1, R) \right|^2}{\left| \bar{\psi}_+(\vartheta, p_e, z_1, R) \right|^2 + \left| \bar{\psi}_-(\vartheta, p_e, z_1, R) \right|^2} \right\}. \quad (17)$$

At each time step t_f, the electron wave packet of H_2^+ is picked out and the fast Fourier transformation is performed to obtain the momentum distribution for the electron,

$$\bar{\psi}_+(\vartheta, p_e, z_1, R) = \frac{1}{\sqrt{2\pi}} \int_{z_0}^\infty dz_2 \ \exp(-ip_e z_2)$$
$$\times \psi(z_1, z_2, R, \vartheta, t_f) \quad \text{for} \quad p_e > 0, \quad (18)$$

$$\bar{\psi}_-(\vartheta, p_e, z_1, R) = \frac{1}{\sqrt{2\pi}} \int_{-\infty}^{-z_0} dz_2 \ \exp(-ip_e z_2)$$
$$\times \psi(z_1, z_2, R, \vartheta, t_f) \quad \text{for} \quad p_e < 0, \quad (19)$$

where $z_0 = 33$ a.u is considered to represent the single ionization for H_2 electron moving on the right side of proton i.e. $H + H^+ + e$ or on the left side of proton i.e. $e + H^+ + H$.

Figure 5 shows the newly calculated asymmetry parameter A_e for a single electron steered in the laser field. I can generally identify two energy regions according to the modulation of the ϑ-dependent A_e. A slight rapid motion of the quivering electron in the laser field for all ϑs generates kinetic energies E_e less than 24 eV. This energy region corresponds to the electron moving in the barrier-less Coulomb potential for small $R < 4$ a.u as depicted in Fig. 4. At this short R, the bound electron follows the laser field adiabatically, tunneling between both sides of H_2^+ as the laser field oscillates leading to the observed strong ϑ-dependent asymmetry modulation. The A_e ranging from -0.4 to 0.4 indicates that the electron is weakly preferential being localized to the left or right of the molecule. Thus the two-fold nearly degenerate of the dressed σ_+ and σ_- states are about equally occupied by the electron population.

The electron in the six-cycle pulse leaves the laser focus with quiver kinetic $U_p = 24$ eV acting as a potential to eject the electron with high velocity. In the field-free, one can steer the ejected electron with a higher E_e starting from 24 eV up to 600 eV. As R stretches to 9 a.u., the corresponding Coulomb potential shows a much higher and wider inner barrier that the electron has less probability to transverse, swinging back and forth between protons after $t = 16$ fs. Depending on ϑ, the strong field can effectively distort the gradient of Coulomb potential along the molecular axis. For $\vartheta = 90°, 180°$, the laser-dressed Coulomb potentials almost resemble that one of the field-free symmetrical Coulomb potentials. One can expect at these phases that the electron motion generates the lowest A_e nearly to 0.

For $\vartheta = 0° - 20°$, the distorted potentials with two field-induced levels of σ_- and σ_+ being the highest occupied molecular orbital (HOMO) and the lowest unoccupied molecular orbital (LUMO) lie in two Coulomb potential wells $z_1 < 0$ and $z_1 > 0$, respectively. As H_2^+ vibrates towards the larger R, the electron can no longer follow the laser field, the separation between molecular levels σ_- and σ_+ increases, where the Stark effect downshifts the σ_- level and up-shifts the σ_+ level by the same amount of energy. Since the barrier height separating the two wells increases considerably, the electron gets trapped, ending its route in the upper potential well. This leads to electron localization and thus dissociative-ionization, and acts as well as the trigger of charge resonance enhanced ionization[66,76–78]. Conversely, the Coulomb potentials for $\vartheta = 180° - 200°$ distort in such a way that the σ_- becomes LUMO and σ_+ becomes HOMO as R separation increases and enhances the opposite mechanism of electron localization being preferentially on the left proton.

To coherently control electron localization in both

σ_- and σ_+ levels, the spatial-temporal overlap between both nuclear wave packets propagating along the electronic states σ_g and σ_u of opposite parity as in Eq. (10) must interfere with each other when they arrive at the same time in the dissociation region such that these two states are nearly degenerate at large Rs where dissociation occurs. Such a spatial-temporal overlap of nuclear wave packets is likely to occur when their kinetic energy distribution is similar.

Increasing R leads to very high kinetic energies of the electron and the asymmetries for those phases remain constant, which indicates the electron moving preferentially in one direction. Above U_p also, the asymmetry modulation exhibits smoothly periodic ϑ-dependence with π periodicity. Previous experimental results show how those dissociative-ionization channels and charge resonance enhanced ionization depend on laser intensity for pulses at 800 nm where the bond-softening channel dominates for low intensity, then the above-threshold dissociation takes over with increasing intensity, and end up with the charge resonance enhanced ionization channel to be the most dominant one for the highest intensity[88].

It is also interesting to find a total asymmetry by integrating out the electron spectra over energies or momenta. For a series of ϑ, I can express the total asymmetry for the electron distribution as

$$A_e^{\text{tot}}(\vartheta) = \frac{P_e^+(\vartheta) - P_e^-(\vartheta)}{P_e^+(\vartheta) + P_e^-(\vartheta)}, \quad (20)$$

where

$$P_e^\pm(\vartheta) = \int_{E_{\min}}^\infty dE_e S_e^\pm(E_e). \quad (21)$$

Inserting Eq. (16) into Eq. (21) to yield

$$P_e^\pm(\vartheta) = \int_{E_{\min}}^\infty dE_e \frac{1}{|p_e|} \int_0^\infty \\ \times dR \int_{-z_0}^{z_0} dz_1 \left| \bar{\psi}_\pm(\vartheta, p_e, z_1, R) \right|^2, \quad (22)$$

while inserting Eq. (22) into Eq. (20), I obtain

$$A_e^{\text{tot}}(\vartheta) = \int_{E_{\min}}^\infty dE_e \frac{1}{|p_e|} \int_0^\infty dR \int_{-z_0}^{z_0} dz_1 \\ \times \left\{ \frac{\left|\bar{\psi}_+(\vartheta, p_e, z_1, R)\right|^2 - \left|\bar{\psi}_-(\vartheta, p_e, z_1, R)\right|^2}{\left|\bar{\psi}_+(\vartheta, p_e, z_1, R)\right|^2 + \left|\bar{\psi}_-(\vartheta, p_e, z_1, R)\right|^2} \right\} \\ = \int_{E_{\min}}^\infty dE_e \frac{1}{|p_e|} A_e(\vartheta, E_e) \quad (23)$$

and $E_{\min} = 0.1$ a.u. for electron. Figure 6 displays A_e^{tot} covering all the kinetic energies gained by the electron, E_e. Apparently, there are two lobes representing the most preferential ionization channels that electron can take place during dissociation, controlled by the fixed ϑ-dependent laser field. As far as the highest possible of A_e^{tot} is concerned, the laser phase can be set up at $\vartheta = 10°$ and $190°$ to yield the most probable right and left ionization channels, respectively.
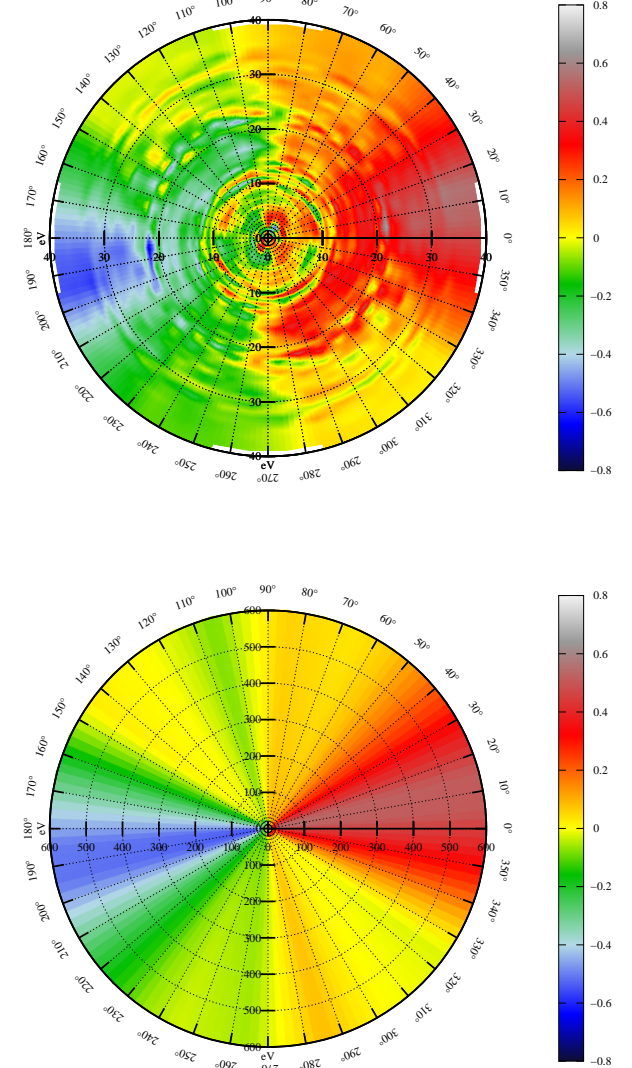

FIG. 5. Asymmetry parameters A_e for the electron localization of H_2^+ at specific energies E_N (in eV) at various laser carrier envelope phases ϑ (in degree).

IV. CONCLUSION

In summary, the nonlinear, non-perturbative interaction of the strong field six-cycle laser pulses with H_2 leads to interesting electron dynamics of H_2^+. Following the first ionization is that the electron distribution gets trapped in the Coulomb potential for about 8 fs before splitting into two ionization channels due to the inner Coulomb potential barrier when H_2^+ stretches to the critical internuclear distance of 4 a.u. Controlling the carrier-envelope phase ϑ allows one to control electron localization. In the laser field, the electron quivers with the laser cycle accordingly, and its directionality in time occurs periodically by $\vartheta + \pi$, which is the main characteristic of the homonuclear diatomic molecule. One striking observation is that as the electron enters into the field-free region, the electron slowly no longer fol-
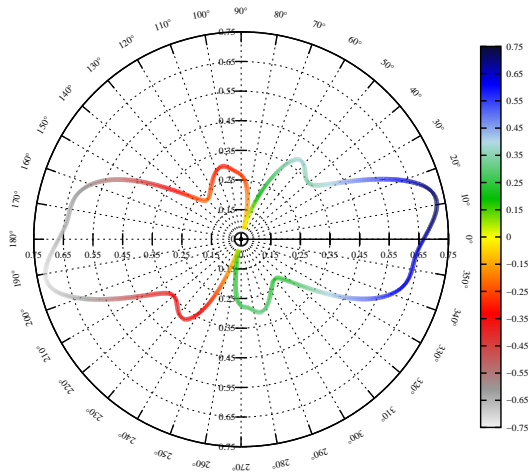
FIG. 6. Total asymmetry parameters A_e^{tot} for the electron localization of H_2^+ over all energies E_N (in eV) at various laser carrier envelope phases ϑ (in degree).

lows the laser oscillation. Depending on the ϑ, the electron eventually gets trapped favorably in one of the two Coulomb potential wells. This asymmetry electron distribution due to the distortion of Coulomb potential occurs after the end of the laser cycle of 24 fs with nuclear separation around 9 a.u. With a full range of ϑ enables one to determine the highest possible total asymmetry A_e^{tot} covering all energies namely at -0.75 and 0.75 by setting up $\vartheta = 10°$ and $190°$, respectively, to represent preferential directionality of electron towards the right or the left side of the H_2^+ molecule. This important part of the works reveals how the laser-controlled electron slightly reorganizes its position accordingly to track the shift in the position of the proton despite much heavier proton's mass compared to electron ones.

ACKNOWLEDGMENTS

[1] A. H. Zewail, J. Phys. Chem. A **104**, 5660 (2000).

[2] T. Brabec and F. Krausz, Rev. Mod. Phys. **72**, 545 (2000).

[3] In *Strong Field Laser Physics*, edited by T. Brabec, (Springer Series in Optical Science, Springer, New York, 2009), Vol. 134.

[4] K. C. Kulander and M. Lewenstein, in *Multiphoton and Strong-Field Processes*, (Springer Handbook of Atomic, Molecular and Optical Physics, Springer Science, New York, 2006).

[5] A. D. Bandrauk, in *Molecules in Laser Fields*, (Marcel Dekker Inc., New York, 1994).

[6] M. H. Mittleman, in *Introduction to the Theory of Laser-Atom Interaction*, (Plenum Press, New York, 1993), 2nd edn.

[7] F. H. M. Faisal, in *Theory of Multiphoton Processes*, (Plenum Press, New York, 1987).

[8] N. B. Delone and V. P. Krainov, in *Multiphoton Processes in Atoms*, (Springer-Verlag, Berlin, 1999).

[9] T. Brabec and F. Krausz, Rev. Mod. Phys. **72**, 545 (2000).

[10] U. Keller, Nature **424**, 831 (2003).

[11] J. Parker and C. W. Clark, J. Opt. Soc. Am. B **13**, 371 (1996)

[12] M. Bashkansky, P. Bucksbaum, and D. Schumacher, Phys. Rev. Lett. **60**, 2458 (1988).

[13] A. Zavriyev, P. H. Bucksbaum, H. G. Muller, and D. W. Schumacher, Phys. Rev. A **42**, 5500 (1990).

[14] A. Giusti-Suzor, X. He, O. Atabek, and F. H. Mies, Phys. Rev. Lett. **64**, 515 (1990).

[15] B. D. Esry, A. M. Sayler, P. Q. Wang, K. D. Carnes, and I. Ben-Itzhak, Phys Rev Lett. **97**, 013003 (2006).

[16] J. L. Krause, K. J. Schafer, and K. C. Kulander, Phys. Rev. Lett. **68**, 3535 (1992).

[17] A. D. Bandrauk , S. Barmaki, and G. L. Kamta, Phys. Rev. Lett. **98**, 13001 (2007).

[18] G. H. C. New and J. F. Ward, Phys. Rev. Lett. **19**, 556 (1967).

[19] N. H. Burnett, H. A. Baldis, M. C. Richardson, and G. D. Enright, Appl. Phys. Lett. **31**, 172 (1977).

[20] P. B. Corkum, Phys. Rev. Lett. **71**, 1994 (1993).

[21] A. Douhal, F. Lahmani, and A. H. Zewail, Chemical Physics, **207**, 477 (1996).

[22] N. A. Papadogiannis, B. Witzel, C. Kalpouzos, and D. Charalambidis, Phys. Rev. Lett. **83**, 4289 (1999).

[23] P. Corkum, Nature **403**, 845 (2000).

[24] V. Roudnev, B. D. Esry, and I. Ben-Itzhak, Phys. Rev. Lett. **93**, 163601 (2004).

[25] G. Sansone, F. Kelkensberg, J. F. Pérez-Torres, F. Morales, M. F. Kling, W. Siu, O. Ghafur, P. Johnsson, M. Swoboda, E. Benedetti, F. Ferrari, F. Lépine, J. L. Sanz-Vicario, S. Zherebtsov, I. Znakovskaya, A. L'Huillier, M. Yu. Ivanov, M. Nisoli, F. Martín, and M. J. J. Vrakking, Nature **465**, 763 (2010).

[26] K. P. Singh, F. He, P. Ranitovic, W. Cao, S. De, D. Ray, S. Chen, U. Thumm, A. Becker, M. M. Murnane, H. C. Kapteyn, I.V. Litvinyuk, and C. L. Cocke, Phys. Rev. Lett. **104**, 023001 (2010).

[27] D. Ray, F. He, S. De, W. Cao, H. Mashiko, P. Ranitovic, K. P. Singh, I. Znakovskaya, U. Thumm, G. G. Paulus, M. F. Kling, I.V. Litvinyuk, and C. L. Cocke, Phys. Rev. Lett. **103**, 223201 (2009).

[28] M. F. Kling, Ch. Siedschlag, A. J. Verhoef, J. I. Khan, M. Schultze, Th. Uphues, Y. Ni, M. Uiberacker, M. Drescher, F. Krausz, and M. J. J. Vrakking, Science **312**, 246 (2006).

[29] G. G. Paulus, F. Grasbon, H. Walther, P. Villoresi, M. Nisoli, S. Stagira, E. Priori, and S. De Silvestri, Nature **414**, 182 (2001).

[30] A. Gürtler, F. Robicheaux, W. J. van der Zande, and L. D. Noordam, Phys. Rev. Lett. **92**, 033002 (2004).

[31] S. Chelkowski, A. D. Bandrauk, and A. Apolonski, Phys. Rev. A **70**, 013815 (2004).

[32] C. Altucci, V. Tosa, R. Velotta, and C. H. Nam, Phys. Rev. A **70**, 065402 (2004).

[33] X. M. Tong, K. Hino, and N. Toshima, Phys. Rev. A **74**, 031405(R) (2006).

[34] T. Nakajima and S.Watanabe, Phys. Rev. Lett. **96**, 213001 (2006).

[35] M. G. Makris and P. Lambropoulos, J. Phys. B **37**, 2247 (2004).

[36] S. X. Hu and L. A. Collins, Phys. Rev. A **73**, 023405 (2006).

[37] C. P. J. Martiny and L. B. Madsen, Phys. Rev. Lett. **97**, 093001 (2006).

[38] A. Kramo, E. Hasović, D. B. Milošević, and W. Becker, Laser Phys. Lett. **4**, 279 (2007).

[39] G. L. Kamta and A. D. Bandrauk, Phys. Rev. Lett. **94**, 203003 (2005).

[40] S. Chelkowski and A. D. Bandrauk, Phys. Rev. A **65**, 061802(R) (2002).

[41] C. Uiberacker and W. Jakubetz, J. Chem. Phys. **120**, 11532 (2004).

[42] A. Baltuska, T. Udem, and M. Uiberacker, Nature **421**, 611 (2003).

[43] J. H. Posthumus and J. F. McCann, Diatomic Molecules in Intense laser Fields, In *Molecules and Clusters in Intense Laser Fields*, edited by J. H. Posthumus (Cambridge University Press, Cambridge, 2001), p. 27.

[44] A. Giusti-Suzor, F. H. Mies, L. F. DiMauro, E. Charron, and B. Yang, J. Phys. B: At. Mol. Opt. Phys. **28**, 309, (1995).

[45] S. T. Cundiff, F. Krausz, and T. Fuji, Carrier-Envelope Phase of Ultrashort Pulses, in *Strong Field Laser Physics*, edited by T. Brabec (Springer Series in Optical Sciences, Springer, New York, 2008), Vol. 134, p. 61.

[46] M. N. Daud, H. Lu, S. Chelkowski, and A. D. Bandrauk, Int. J. Quantum Chem. **115**, 369 (2015).

[47] M. F. Kling, A. J. Verhoef, J. I. Khan, M. Schultze, Y. Ni, M. Uiberacker, M. Drescher, F. Krausz, and M. J. J. Vrakking, Science **312**, 246 (2006).

[48] V. Wanie, H. Ibrahim, S. Beaulieu, N. Thiré, B. E. Schmidt, Y. Deng, A. S. Alnaser, I. V. Litvinyuk, X.-M.Tong, and F. Légaré, J. Phys. B: At. Mol. Opt. Phys. **49**, 25601 (2016).

[49] I. Znakovskaya, P. von den Hoff, G. Marcus, S. Zherebtsov, B. Bergues, X. Gu, Y. Deng, M. J. J. Vrakking, R. Kienberger, F. Krausz, R. de Vivie-Riedle, and M. F. Kling, Phys. Rev. Lett. **108**, 63002 (2012).

[50] M. D. Feit, J. A. Fleck Jr., and A. Steiger, J. Comput. Phys. **47**, 412 (1982).

[51] M. N. Daud, Int. J. Quantum Chem. **116**, 452 (2016).

[52] M. N. Daud, Eur. Phys. J. D **68**, 267 (2014).

[53] M. N. Daud, G. G. Balint-Kurti, and A. Brown, J. Chem. Phys **122**, 054305 (2005).

[54] M. N. Daud, submitted.

[55] X. Urbain, B. Fabre, E. M. Staicu-Casagrande, N. de Ruette, V. M. Andrianarijaona, J. Jureta, J. H. Posthumus, A. Saenz, E. Baldit, and C. Cornaggia, Phys. Rev. Lett. **92**, 163004 (2004).

[56] M. Meckel, D. Comtois, D. Zeidler, A. Staudte, D. Pavicic, H. C. Bandulet, H. Pépin, J. C. Kieffer, R. Dörner, D. M. Villeneuve, P. B. Corkum, Science **320**, 1478 (2008).

[57] T. Nubbemeyer, K. Gorling, A. Saenz, U. Eichmann, and W. Sandner, Phys. Rev. Lett. **101**, 233001 (2008).

[58] P. Eckle, A. N. Pfeiffer, C. Cirelli, A. Staudte, R. Dörner, H. G. Muller, M. Büttiker, and U. Keller, Science **322**, 1525 (2008).

[59] A. Saenz, Phys. Scr. **T110**, 126 (2004).

[60] A. Saenz, Phys. Rev. A **66**, 63407 (2002).

[61] P. H. Bucksbaum, A. Zavriyev, H. G. Muller, and D. W. Schumacher, Phys. Rev. Lett. **64**, 1883 (1990).

[62] P. H. Bucksbaum, A. Zavriyev, H. G. Muller, and D. W. Schumacher, Phys. Rev. Lett. **64**, 1883 (1990).

[63] A. Giusti-Suzor, X. He, O. Atabek, and F. H. Mies, Phys. Rev. Lett. **64**, 515, (1990).

[64] A. Zavriyev, P. H. Bucksbaum, H. G. Muller, and D. W. Schumacher, Phys. Rev. A **42**, 5500, 1990.

[65] G. Jolicard and O. Atabek, Phys. Rev. A **46**, 5845, (1992).

[66] A. D. Bandrauk and M. L. Sink, J. Chem. Phys. **74**, 1110 (1981).

[67] A. Zavriyev, P. H. Bucksbaum, J. Squier, and F. Saline, Phys. Rev. Lett. **70**, 1077 (1993).

[68] L. J. Frasinski, J. H. Posthumus, J. Plumridge, K. Codling, P. F. Taday, and A. J. Langley, Phys. Rev. Lett. **83**, 3625 (1999).

[69] L. J. Frasinski, J. Plumridge, J. H. Posthumus, K. Codling, P. F. Taday, E. J. Divall, and A. J. Langley, Phys. Rev. Lett. **86**, 2541 (2001).

[70] E. E. Aubanel, J. M. Gauthier, and A. D. Bandrauk, Phys. Rev. A **48**,2145 (1993).

[71] A. Giusti-Suzor and F. H. Mies, Phys. Rev. Lett. **68**, 3869 (1992).

[72] G. H. Yao and S. I. Chu, Chem. Phys. Lett. **197**, 413 (1992).

[73] F. Légaré, I. Litvinyuk, P. Dooley, F. Quéré, A. Bandrauk, D. Villeneuve, and P. Corkum, Phys. Rev. Lett. **91**, 93002 (2003).

[74] F. Légaré, K. F. Lee, A. D. Bandrauk, D. M. Villeneuve, and P. B. Corkum, J. Phys. B: At. Mol. Opt. Phys. **39**, S503 (2006).

[75] H. Xu, Z. Li, F. He, X. Wang, A. Atia-Tul-Noor, D. Kielpinski, R. T. Sang, and I. V. Litvinyuk, Nat. Commun. **8**, 15849 (2017).

[76] T. Seideman, M. Y. Ivanov, and P. B. Corkum, Phys. Rev. Lett. **75**, 2819 (1995).

[77] A. D. Bandrauk and H. Lu, J. Mol. Struct. Theochem. **547**, 97 (2001).

[78] H. Liang, X.-R. Xiao, Q. Gong, and L.-Y. Peng, J. Phys. B: At. Mol. Opt. Phys. **50**, 174002 (2017).

[79] H. Li, A. S. Alnaser, X. M. Tong, K. J. Betsch, M. Kübel, T. Pischke, B. Förg, J. Schötz, F. Süβmann, S. Zherebtsov, B. Bergues, A. Kessel, S. A. Trushin, A. M. Azzeer, and M. F. Kling, J. Phys. B: At. Mol. Opt. Phys. **47**, 124020 (2014).

[80] M. Kremer, B. Fischer, B. Feuerstein, V. L. B. de Jesus, V. Sharma, C. Hofrichter, A. Rudenko, U. Thumm, C. D. Schröter, R. Moshammer, and J. Ullrich, Phys. Rev. Lett. **103**, 213003 (2009).

[81] H. Xu, J.-P. Maclean, D. E. Laban, W. C. Wallace, D. Kielpinski, R. T. Sang, and I. V. Litvinyuk, New J. Phys. **15**, 23034 (2013).

[82] X. Gong, P. He, Q. Song, Q. Ji, H. Pan, J. Ding, F. He, H. Zeng, and J. Wu, Phys. Rev. Lett. **113**, 203001 (2014).

[83] Z. Wang, K. Liu, P. Lan, and P. Lu, Phys. Rev. A **91**, 43419 (2015).

[84] H. Xu, H. Hu, X.-M. Tong, P. Liu, R. Li, R. T. Sang, and I. V. Litvinyuk, Phys. Rev. A **93**, 63416 (2016).

[85] G. Sansone, F. Kelkensberg, F. Morales, F. Mart, and M. J. J. Vrakking, IEEE J. Sel. Top. Quantum Electron. **18**, 520 (2012).

[86] V. Roudnev and B. D. Esry, Phys. Rev. Lett. **99**, 220406 (2007).

[87] P. Brumer and M. Shapiro, Ann. Rev. Phys. Chem. **43**, 257 (1992).

[88] A. Alnaser, X. Tong, T. Osipov, S. Voss, C. Maharjan, B. Shan, Z. Chang, and C. Cocke, Phys. Rev. A **70**, 23413 (2004).